Alteration of the cholinergic system and motor deficits in cholinergic neuron-specific *Dyt1* knockout mice

Yuning Liu[1,2], Hong Xing[1], Wanhui Sheng[4], Kyle N Singh[1], Alexandra G. Korkmaz[1], Caroline Comeau[1], Maisha Anika[1], Alexis Ernst[1], Fumiaki Yokoi[1], David E. Vaillancourt[3], Charles J. Frazier[4], Yuqing Li[1,2,*]

[1]Norman Fixel Institute for Neurological Diseases, Department of Neurology, College of Medicine, University of Florida, Gainesville, FL, United States

[2]Genetics Institute, University of Florida, Gainesville, FL, United States

[3]Department of Applied Physiology and Kinesiology, Biomedical Engineering, and Neurology, University of Florida, Gainesville, FL, United States

[4]Department of Pharmacodynamics, College of Pharmacy, University of Florida, Gainesville, FL, United States.

Abstract

Dystonia is a neurological movement disorder characterized by sustained or intermittent muscle contractions, repetitive movement, and sometimes abnormal postures. DYT1 dystonia is one of the most common genetic dystonias, and most patients carry heterozygous *DYT1* ΔGAG mutations causing a loss of a glutamic acid of the protein torsinA. Patients can be treated with anticholinergics, such as trihexyphenidyl, suggesting an abnormal cholinergic state. Early work on the cell-autonomous effects of *Dyt1* deletion with ChI-specific *Dyt1* conditional knockout mice (*Dyt1* Ch1KO) revealed abnormal electrophysiological responses of striatal ChIs to muscarine and quinpirole, motor deficits, and no changes in the number or size of the ChIs. However, the *Chat-cre* line that was used to derive *Dyt1* Ch1KO mice contained a neomycin cassette and was reported to have ectopic *cre*-mediated recombination. In this study, we generated a *Dyt1* Ch2KO mouse line by removing the neomycin cassette in *Dyt1* Ch1KO mice. The *Dyt1* Ch2KO mice showed abnormal paw clenching behavior, motor coordination and balance deficits, impaired motor learning, reduced striatal choline acetyltransferase protein level, and a reduced number of striatal ChIs. Furthermore, the mutant striatal ChIs had a normal muscarinic inhibitory function, impaired quinpirole-mediated inhibition, and altered current density. Our findings demonstrate a cell-

*Correspondence to Dr. Yuqing Li, Department of Neurology, College of Medicine, University of Florida, PO Box 100236, Gainesville, FL 32610-0236, USA. yuqing.li@neurology.ufl.edu.

autonomous effect of *Dyt1* deletion on the striatal ChIs and a critical role for the striatal ChIs and corticostriatal pathway in the pathogenesis of DYT1 dystonia.

Keywords

DYT1; dystonia; the cholinergic system; torsinA; ChAT

1. Introduction

Dystonia is a neurological movement disorder characterized by sustained or intermittent muscle contractions, repetitive movement, and sometimes abnormal postures (Albanese et al., 2013). DYT1 or DYT-TOR1A dystonia is the most common type of early-onset generalized dystonia (Bressman et al., 2000; Marras et al., 2016) with symptom onset from 5 to 28 years old. It is an autosomal dominant disease with low penetrance (30%–40%), possibly caused by additional genetic or environmental factors (Kock et al., 2006; Opal et al., 2002; Risch et al., 1995; Yokoi et al., 2010). The individuals affected by DYT1 dystonia frequently have a heterozygous three base-pair (*GAG*) deletion located in exon 5 of *DYT1* or *TOR1A*, leading to a loss of one glutamate residue for torsinA (E-torsinA) (Ozelius et al., 1997). Recent reports demonstrated homozygous mutation in *DYT1* causes arthrogryposis, tremor, developmental delay, and motor deficits (Isik et al., 2019; Kariminejad et al., 2017; Reichert et al., 2017).

TorsinA is a member of the AAA+ (ATPase associated with a variety of cellular activities) superfamily (Ozelius et al., 1997). It is expressed highly during early brain development (Siegert et al., 2005; Vasudevan et al., 2006; Xiao et al., 2004), especially within the neurons located in the basal ganglia, cerebral cortex, hippocampus, thalamus, and cerebellum (Augood et al., 1999; Shashidharan et al., 2000). In DYT1 patients, mutant torsinA might exert a dominant-negative effect and decrease wildtype torsinA activity due to a homo-oligomeric feature of AAA + proteins (Konakova and Pulst, 2005; Pham et al., 2006). Several crystal structural studies (Brown et al., 2014; Demircioglu et al., 2016; Zhao et al., 2013) demonstrated that the E-torsinA mutation alters helix $\alpha 7$ at the interface with interacting partners, leading to the reduced interaction between torsinA and LAP1/LULL1, and the loss of ATP hydrolysis ability (Chase et al., 2017).

The striatum is the main component of the basal ganglia and functions in regulating movement and cognition based on the balanced modulation of striatal synaptic circuits between ChIs and the axon terminals from the dopaminergic neurons of the substantia nigra (Aosaki et al., 2010; Pisani et al., 2007; Stoof et al., 1992). Striatal cholinergic transmission is mediated primarily by large aspiny striatal ChIs. The striatal cholinergic system plays a critical role in the pathophysiology of DYT1 dystonia (Eskow Jaunarajs et al., 2015). Anticholinergic drugs, such as trihexyphenidyl, are clinically effective in treating DYT1 dystonia (Jankovic, 2013). ChIs have an autoregulation mechanism. ACh or muscarine, a muscarinic ACh receptor agonist, can reduce the spontaneous firing of ChIs through the muscarinic M2/M4 receptors (Ding et al., 2006; Howe and Surmeier, 1995; Yan and Surmeier, 1996). Moreover, dopamine (DA) or quinpirole, a D2R agonist, binds to dopamine

D2 receptor (D2R) on dorsal striatal ChIs and suppresses its spontaneous firing (Chuhma et al., 2014; Maurice et al., 2004). Interestingly, paradoxical excitation of striatal ChIs in quinpirole response has been reported in multiple genetic models of DYT1 dystonia (Grundmann et al., 2012; Martella et al., 2014; Scarduzio et al., 2017; Sciamanna et al., 2012; Sciamanna et al., 2011). There is also a lack of response to muscarine in *Dyt1* Ch1KO mice (Sciamanna et al., 2012). Furthermore, two independent *Dyt1* knock-in models with the trinucleotide deletion seen commonly in DYT1 patients have been developed (Dang et al., 2005; Goodchild et al., 2005). The knock-in mice have impaired corticostriatal long-term depression (LTD), beam-walking deficits and co-contractions of the antagonistic muscle, which can be rescued by anticholinergic drugs (Dang et al., 2012; DeAndrade et al., 2016; Martella et al., 2014). Finally, *Dyt1* knock-in mice have increased extracellular ACh (Downs et al., 2019; Scarduzio et al., 2017). These findings suggest an altered cholinergic system in DYT1 dystonia.

Tissue- and cell type-specific *Dyt1* conditional KO mice are useful in understanding the pathophysiology of the DYT1 dystonia. Previously, a cholinergic cell-specific *Dyt1* conditional KO mouse line (*Dyt1* Ch1KO) was generated to investigate what pathological role torsinA plays in ChIs (Sciamanna et al., 2012). There is no loss of striatal ChIs in the *Dyt1* Ch1KO mice. On the other hand, the *Dyt1* Ch1KO mice exhibit motor deficits in the rotarod test and loss of muscarinic and D2R inhibitory function in the striatal ChIs. However, the *Chat-cre* mice (Stock No: 006410, The Jackson Lab) used to generate *Dyt1* Ch1KO have the neomycin cassette and was reported to have ectopic *cre* expression, especially in astrocytes (Hedrick et al., 2016; Nasirova et al., 2020). Separately, the forebrain- and cholinergic neuron-specific *Dyt1* KO (Dlx-CKO/ mice and ChAT-CKO/ mice) both show a reduced number of dorsal striatal ChIs and severe motor and postural abnormalities (Pappas et al., 2015; Pappas et al., 2018). However, these two models both have one *Dyt1* allele removed throughout the whole body, the effect of which is unknown. Here, we attempt to address the three existing mouse models' discrepancies on behavior and striatal ChI numbers. We developed and characterized a new ChI-specific *Dyt1* KO mouse model (*Dyt1* Ch2KO) by removing the neomycin cassette in the *Dyt1* Ch1KO mice.

2. Materials and methods

The IACUC at the University of Florida approved all animal experiments in compliance with the USPHS Guide for Care and Use of Laboratory Animals. Experiments were carried out by investigators blind to the genotypes. The mice were housed with *ad libitum* access to food and water under the condition of 12 hours-light and 12 hours-dark.

2.1. Animals

Chat-cre mice or *Ch1cre* mice were purchased from Jackson Laboratory (Stock No: 006410; ChAT-IRES-Cre::*frt*-neo-*frt*) (Rossi et al., 2011). To remove the neomycin cassette, we imported the FLP strain (Stock No: 003946; ROSA26::FLPe knock-in) (Farley et al., 2000) and backcrossed with C57BL/6 background for at least six generations. The FLP mice were then bred with *Ch1cre* mice to generate the *Chat-cre- neo* mice or *Ch2cre* mice. The FLP locus was removed for subsequent breedings. To validate the Cre recombinase activity, we

generated *Ch2cre*-GFP mice by crossing *Ch2cre* mice with GFP-Cre reporter line (Stock No: 007906; Rosa26-CAG promoter-loxP-STOP-loxP-ZsGreen) (Madisen et al., 2010). *Dyt1*^{loxP} mice, which contain floxed exons 3–4 in the *Dyt1* gene, were prepared as previously described (Yokoi et al., 2008). *Ch2cre* +/– *Dyt1*$^{loxP/+}$ mice (DHet) were generated by crossing the *Ch2cre* +/– mice and *Dyt1*$^{loxP/loxP}$ mice. *Dyt1* Ch2KO mice and their control (CT) littermates (*Dyt1*$^{loxP/loxP}$ or *Dyt1*$^{loxP/+}$) were generated by crossing the DHet mice with *Dyt1*$^{loxP/loxP}$ mice. Genotyping for Ch2KO mice was performed by multiplex PCR using a set of Dyt1loxpF (5_-GAGGAGAAAATAGGGGCTCAGTAT-3_) and Dyt1loxpR (5_-GAAGGTTGAGAAACTGCCTTAGAG-3_) primers for *Dyt1*^{loxP}; a set of creA (5_-ATCTCCGGTATTGAAACTCCAGCGC-3_) and cre6 (5_-CACTCATGGAAAATAGCGATC- 3_) primers for *cre* (Yokoi et al., 2012). Earlier studies of DYT1 dystonia mouse models show behavioral and neurochemical changes in the male mice only (Dang *et al.*, 2005; Dang *et al.*, 2006; Yokoi *et al.*, 2020). Therefore, we only used male mice in the current studies unless specified otherwise.

2.2. Fluorescence immunohistochemistry (FIHC)

Adult male *Ch2cre*-GFP mice (n=2) were sacrificed and perfused with ice-cold 0.1M phosphate buffer (PB; pH 7.4) followed with 4% paraformaldehyde in 0.1M phosphate-buffered saline (PBS; pH 7.4). The brains were incubated with the fixative overnight and then with 30% sucrose in 0.1 M PB until the brain sank. Each brain was frozen with dry-ice powder, and coronal sections with 40 μm thickness were prepared using a freezing sliding microtome. The brain slices containing the striatum were selected. The free-floating brain sections were washed three times in 10 mM glycine/0.1 M PB for 5 min each and blocked in 2% gelatin/0.1 M PB for 15 min, 10 mM glycine/0.1 M PB for 5 min and 0.1% BSA/0.1M PB for 5 min. The treated slices were incubated in goat anti-choline acetyltransferase (ChAT) antibody (EMD Millipore, AB144P; 1:50 dilution) in 1% BSA/0.1 M PB for 2 hours and washed in 0.1% BSA/0.1 M PB for 5 min each, six times. The slices were then incubated with Alexa Fluor 594 donkey anti-goat IgG (H+L) (Invitrogen, A11058; 1:200 dilution) in 1% BSA/0.1 M PB for 2 hours and then washed in 0.1% BSA/0.1 M PB for 5 min each, six times. The slices were mounted on glass slides with Vectashield Hard Set mounting medium for fluorescence (Vector Lab Inc., H-1400), covered with cover glass and stored at 4°C overnight. The double-positive cells were counted using a ZEISS Axiophot RZGF-1 microscope with Plan-NEOFLUAR objective lens, and FITC filter for GFP and Texas Red filter for Alexa Fluor 594, and digitized using Neurolucida 7 and NeuroExplorer software (MicroBrightFields Bioscience).

2.3. Immunohistochemistry (IHC) and cell counting

To count the striatal ChI numbers, we perfused and sliced 3 pairs of male *Dyt1* Ch2KO, DHet, and CT littermates at 5 months of age and 4 pairs of male *Dyt1* Ch2KO and 3 CT littermates at 13 months of age as described above. Every sixth section was stained with goat anti-ChAT antibody (EMD Millipore, AB144P; 1:100 dilution; Vectastain ABC kit for peroxidase goat IgG and DAB peroxidase substrate kit, Vector Laboratories). The microscope images were captured by the Neurolucida program. The striatal area of the image was quadrisected to dorsolateral (DL), dorsomedial (DM), ventral lateral (VL), and ventral medial (VM) areas, i.e., it was vertically bisected at the midpoint of the corpus

callosum and horizontally bisected halfway between the corpus callosum and the anterior commissure (Pappas et al., 2015). The number of ChAT-positive neurons in the striatum were counted. The ChI density was calculated and expressed as the number of ChIs per mm^2.

2.4. Western blot analysis

Six male *Dyt1* Ch2KO and eight CT littermates about 4 months of age, and seven male *Dyt1* Ch2KO and six CT littermates at 13 months of age were used for Western blot analysis. The striata were dissected and homogenized in 200 μl of ice-cold lysis buffer, and the proteins were extracted in 1% Triton X-100-containing buffer and quantified as previously described (Yokoi et al., 2010). Protein samples were separated on 10% sodium dodecyl sulfate-polyacrylamide gel electrophoresis (SDS-PAGE) and transferred to Millipore Immobilon-FL transfer PVDF membranes. The membranes were blocked with LI-COR Odyssey blocking buffer and incubated at 4°C overnight with goat anti-ChAT antibody (EMD Millipore, AB144P; 1:1,000 dilution) and rabbit anti-glyceraldehyde-3-phosphate dehydrogenase (GAPDH) antibody (Santa Cruz, sc-25778; 1:1,000 dilution). LI-COR IRDye 800CW donkey anti-goat IgG (H+L) or LI-COR IRDye 680RD donkey anti-rabbit IgG (H+L) were used when appropriate at the dilution of 1:15,556. The signals were detected with an LI-COR Odyssey imaging system. The density of the corresponding protein band was normalized to those of GAPDH. Western blot analysis was performed in duplicate.

2.5. Electrophysiology

Electrophysiological recordings of ChIs were obtained from 15 *Dyt1* Ch2KO and 15 CT littermates (6 pairs of female and 9 pairs of male mice) with an average age of 6 months. Slice preparation, ChI identification, and cell-attached recording were performed as described previously (Lyu et al., 2019). Briefly, the mouse was anesthetized via isoflurane inhalation and subsequently decapitated. The brain was rapidly extracted. Coronal brain slices (300 μm) containing the dorsal striatum were cut inside a chamber filled with ice-cold, oxygenated cutting saline using a Vibratome (Leica VT 1000s). The cutting saline solution concentrations were (in mM): 180 Sucrose, 2.5 KCl, 1.25 NaH_2PO_4, 25 $NaHCO_3$, 1 $CaCl_2$, and 10 $MgCl_2$, 10 D-glucose. The slices were recovered for 60 minutes at 35°C in a holding chamber with oxygenated artificial cerebrospinal fluid (ACSF). The ACSF solution concentrations were (in mM): 126 NaCl, 2.5 KCl, 1.25 NaH_2PO_4, 25 $NaHCO_3$, 2 $MgCl_2$, 1 $CaCl_2$, and 10 D-glucose. The slices were then incubated at room temperature until electrophysiological recording.

The slices were visualized with an upright microscope (Zeiss, Germany) using a 40× water-immersion objective with infrared optics. Cholinergic interneurons were identified based on morphology and size, as they are irregularly polygonal with large cell soma (>20 μm), and were further confirmed by characteristic electrophysiological properties observed in whole-cell current-clamp recordings (Oswald et al., 2009). Electrodes for cell-attached and whole-cell recordings were filled with a K-gluconate-based solution containing the following solutions (in mM): 112.5 K-gluconate, 4 NaCl, 17.5 KCl, 0.5 CaCl2, 5 MgATP, 1 NaGTP, 5 EGTA, 10 HEPES; with pH of 7.2 (270–280 mOsm) and resistance of 5–10 MΩ. Positive pressure was applied to the patch electrode as it approached the cholinergic interneuron.

Suction was applied to the electrode to create a seal (> 5 GΩ) between the recording pipette and cell membrane. After breaking through the cell membrane, the whole-cell recording was performed to obtain intrinsic properties and the effect of the muscarine in the voltage-clamp configuration. The analysis of whole-cell recording data was performed using custom software written in OriginC (OriginLab) by CJF. Cells were excluded from data analysis if the access resistance (Ra) exceeded 40 Mohm, and a small number of individual measurements in the intrinsic properties datasets were masked if they were greater than two standard deviations from the mean. In voltage-clamp configuration, input resistance (Rm) was calculated as [ΔV − (Ra*I_{SS})]/I_{SS}, where I_{SS} is the steady-state current obtained at the end of the 50-msec voltage step from −70 mV to −80 mV. Whole-cell capacitance (Cm) was calculated using data obtained from a 100-msec V-shaped voltage-clamp ramp protocol, repeated for 40 sweeps for each cell, where the ramp starts from −70 mV, descends to −80 mV, and ascends back to −70mV (0.2 mV/msec in both directions). Specifically, Cm was calculated as (ΔI/2)/(ΔV/Δt), where ΔI is the average difference in current observed during the rising and falling phase of the voltage ramp, and ΔV/Δt is the slope of the voltage command (Cirino et al., 2020; Golowasch et al., 2009). The current density was calculated as I_{Hold}/Cm, where I_{Hold} is the holding current necessary to clamp the cell at −70 mV (Fig. 3C) or at a series of subthreshold voltages (Fig. 3D). In Fig. 4H, Δ current density was defined as the difference in current density (at −70 mV) observed 0–300 seconds before and 150–210 seconds after bath application of muscarine (10 μM). The resting membrane potential was defined as the average voltage observed over a 1 second period in the current clamp with I = 0, when cells were quiescent. Ih mediated voltage change was quantified as the difference between the minimum and steady state voltage observed during a −200 pA current step (from I = 0, 300 msec in duration). All the action potential properties presented in Table 1 were calculated from the first action potential observed during a slow current ramp (≈ 10 pA/s, injected from I = 0 in current clamp until the first action potential was observed). The maximum rate of depolarization and repolarization were obtained from the first derivative of the action potential. Action potential threshold was defined as the voltage at which the depolarization rate first exceeded 5% of the maximum, while the rheobase was defined as the command current at the time of threshold. The amplitude of the afterhyperpolarization (AHP) observed after the first action potential was obtained by subtracting the minimum voltage observed in the 15 ms following the action potential peak from the threshold voltage. Action potential amplitude was calculated as the difference between the threshold voltage and the peak voltage. Action potential width was defined as the time between the observed maximum rate of depolarization and repolarization.

Spontaneous firing in Fig. 4A, 4D and 4F were recorded in cell-attached mode (Lyu et al., 2019), and action potentials were detected using MiniAnalysis (Synaptosoft). Spontaneous firing frequency in ChIs was evaluated both before and after bath application of muscarine (10 μM, 90 seconds). After the drug application, the muscarine was washed out with ACSF. The firing rates 30 seconds before muscarine treatment and 180–210 seconds after the onset of muscarine application were used to quantify the effects. To further test the response to the muscarine, we recorded ChIs in the whole-cell current-clamp configuration (Fig. 4E). Muscarine (10 μM) was bath-applied for 90 seconds and was washed out with ACSF until the cell was completely recovered. Cells were excluded from data analysis if the recorded

cell was resealed during recording. One individual cell was removed due to its greater than two standard deviations from the mean ($p < 0.01$, Grubbs' test). The firing rates 30 seconds before muscarine treatment and 180–210 seconds after the onset of muscarine application were used to quantify the effects. ChIs were separately investigated with bath applications of quinpirole (10 μM, 120 seconds) for testing the effect of agonists to D2R on the ChIs. The firing rates 30 seconds before quinpirole treatment and 60–90 or 180–210 seconds after the onset of quinpirole application were used to quantify the effects.

All experiments were conducted at $32 \pm 0.5°C$ by Warner TC-344B Dual Automatic Temperature Controller (Warner Instruments, Holliston, MA). Cell-attached and whole-cell recordings were obtained from cholinergic interneurons using Axopatch 1D Amplifier (Molecular Devices). Electrophysiological recording data were acquired using pCLAMP 10 software (Molecular Devices). Signals were filtered at 5 kHz and digitized at 10 kHz with a DigiData 1440 (Molecular Devices).

2.6. Behavioral analysis

Motor behaviors were assessed by semi-quantitative assessments, open field, accelerated rotarod tests, beam-walking, and tail hang. Behavioral semi-quantitative assessments of motor disorders were performed as described earlier (Dang et al., 2005; Fernagut et al., 2002). A group of 13 male *Dyt1* Ch2KO and 13 CT littermates around 5 months of age were placed individually on the table. Truncal dystonia and balance adjustments to a postural challenge were examined. Truncal dystonia was assessed as the flexed posture. The postural challenge was observed by flipping the mouse onto its back, and its capability of righting was noted.

The open-field test was performed next during the light period, as previously described (DeAndrade et al., 2012). Each mouse in the same group was placed in the center of a VersaMax Legacy open field apparatus connected to a computerized Digiscan System (Accuscan Instruments, Inc. OH) and continuously monitored for 30 minutes at 1-minute intervals. Bright illumination (approximately 1k lux at the center by a 60W white bulb) was focused on the center of each field.

The accelerated rotarod test assesses the ability of mice to maintain balance and coordination on an accelerating rotating rod. The motor performance of 14 male *Dyt1* Ch2KO and 11 CT littermates at 7 months of age was examined with an accelerating rotarod (Ugo Basile) as previously described (Sciamanna et al., 2012). The apparatus started at an initial speed of 4 rpm, and then each mouse was put on the same slot one by one. The rod speed was gradually accelerated at a rate of 0.2 rpm/s. The latency to fall was measured with a cutoff time of 3 min at a final rate of 40 rpm. Mice were tested for three trials on each day for 2 days. The trials within the same day were performed at about 1-hour intervals.

The beam-walking test was performed next within the last 8 h of the light period after acclimation to a sound-attenuated testing room for 1-hour as described earlier (Dang et al., 2005). 14 male *Dyt1* Ch2KO and 11 CT littermates at 9 months of age were trained to transverse a medium square beam (14 mm wide) in three consecutive trials each day for 2 days. They were tested twice each on the medium square beam and a medium round beam

(17 mm diameter) on the third day. The mice were then tested twice each on a small round beam (10 mm diameter) and a small square beam (7 mm wide) on the fourth day. The number of hind paw slips on each side was counted by investigators blind to the genotypes. All 4 beams were 100 cm long, and the slips traversing the middle 80 cm were counted.

Finally, the tail hang test has been used for evaluating dystonic postures in other genetic mouse models (Liang et al., 2014; Pappas et al., 2015; Pappas et al., 2018). 14 male *Dyt1* Ch2KO and 11 CT at 13 months of age were examined. In brief, each mouse was suspended by its tail and videotaped for 30 seconds. The presence or absence of limb clasping or paw clenching was assessed during these 30 seconds. Limb clasping was defined as the sustained abnormal posture for 2 seconds or more, with the paw either forcefully extended in the air, around the tail, or held tightly against the body. Paw clenching was defined as the clenching of the paws. The presence of paw clenching and its severity were quantified using a scale: 0 = no paw clenching, 1 = mild paw clenching, and 2 = severe paw clenching. The videos were assessed by an observer who was blind to the genotype.

2.7. Statistics

All data were tested for normality using the SAS statistical package. The Western blot signals were analyzed using the student's t-test. The number of the immuno-positive neurons, area, and the densities of the immuno-positive cells (cell/mm^2) in IHC were analyzed by mixed model for normally distributed data or GENMOD procedure with log link for gamma distribution when they were not normally distributed (Yokoi et al., 2020). The age and Atlas plate number (Franklin and Paxinos, 2008) were used as a covariate. For intrinsic properties displayed as a single measure across mutant and control ChIs, a two-tailed, two-sample unpaired student's t-test was used. Welch's correction was used when the population variances were unequal. Repeated measures two-way ANOVA was used to compare current density-voltage relationships and AP gain function between mutant and control ChIs. A paired two-sample t-test was used to evaluate the effect of muscarine on current density in each group. To compare the amplitude of muscarine effect on current density between groups, we applied a two-tailed, two-sample unpaired student's t-test. Drug application of spontaneous firing was analyzed by either mixed model for normally distributed data or GENMOD procedure for not normally distributed data. The recorded neurons were nested within each animal. The age was used as a covariate. Horizontal activity in the open field and latency to fall in the accelerated rotarod test were not normally distributed and were analyzed using the GENMOD procedure (SAS). Vertical activity in the open field test was normally distributed and, therefore, was analyzed by the mixed procedure. Slip numbers in the beam-walking test for the last 3 beams were analyzed using the GENMOD procedure with log link for negative binomial distribution (Dang et al., 2005). The severities of paw clenching in the tail hang test were analyzed by ordinal logistic regression in SPSS using the PLUM procedure (Zambelli et al., 2012). Age and body weight were used as covariates in all behavioral analyses. Significance was assigned at p 0.05.

3. Results

3.1. Generation of *Dyt1* Ch2KO mice

Dyt1 Ch2KO mice were generated to examine the *in vivo* function of torsinA in the cholinergic neurons. *Ch2cre* mice were generated by crossing *Ch1cre* (Rossi et al., 2011) with FLP mice (Farley et al., 2000) (Fig. 1A) to remove the *neomycin* cassette (Fig. 1D1). To validate the Cre recombinase activity, we generated *Ch2cre*-GFP mice by crossing *Ch2cre* mice with a Cre reporter line (Madisen et al., 2010), which expresses the enhanced GFP following Cre-mediated recombination. The Cre recombinase activity was analyzed by counting the overlap of ChAT-positive neurons (red) in FIHC (Fig. 1B1) with the GFP-positive neurons (green) (Fig. 1B2). Among the 100 GFP-positive neurons counted in *Ch2cre*-GFP mice, all were positive for ChAT in *Ch2cre*-GFP mice. The FIHC results confirmed highly efficient Cre-mediated recombination restricted to the striatal ChIs.

Dyt1 Ch2KO mice were generated as described (Figure 1C) and obtained with Mendelian distribution (Supplemental Table 1), suggesting that *Dyt1* Ch2KO mice are neither embryonic nor neonatal lethal. *Dyt1* Ch2KO mice grew up to adulthood with no apparent developmental delay.

3.2. Alteration of the striatal cholinergic system and reduced striatal ChIs in Ch2KO mice

To examine whether selective *Dyt1* deletion in ChIs leads to an altered striatal cholinergic system, we performed a western blot to measure the protein level of the striatal ChAT, the enzyme responsible for the synthesis of ACh. The striatal ChAT level in *Dyt1* Ch2KO mice was significantly reduced to 67% at 4 months of age (Fig. 2A, CT: n = 8 mice; Ch2KO: n = 6 mice, $p = 0.0014$, student's t-test), and to 61% at 13 months of age (Fig. 2A, CT: n = 6 mice; Ch2KO: n = 7 mice, $p = 0.015$, student's t-test). To determine the cause of ChAT reduction, we analyzed the density of the striatal ChIs by measuring the area size of the striatum and counting the striatal ChAT-positive neurons using IHC (Fig. 2B). *Dyt1* Ch2KO mice (n = 3 mice, 5 months of age) had similar number of ChAT-positive neurons in the striatum (Fig. 2C, CT and Ch2KO: $p = 0.70$; CT and DHet: $p = 0.54$; Ch2KO and DHet: $p = 0.33$, Mixed model) and similar striatal area sizes compared with both CT (n = 3) and DHet littermates (n = 3; Fig. 2D, CT and Ch2KO: $p = 0.16$; CT and DHet: $p = 0.25$; Ch2KO and DHet: $p = 0.62$, GENMOD with a gamma distribution). There was a significant reduction in the density of ChAT-positive neuron in Ch2KO mice compared with CT and DHet (Fig. 2E, CT and Ch2KO: $p = 0.006$; CT and DHet: $p = 0.62$; Ch2KO and DHet: $p = 0.042$, GENMOD with a gamma distribution), suggesting reduced striatal ChIs in *Dyt1* Ch2KO. To test the regional distribution of the reduced ChIs in *Dyt1* Ch2KO, we divided the striatal ChIs into 4 quadrants according to the level of the anterior commissure (Fig. 2B), and counted the number of ChAT-positive neurons in each quadrant of the striatum. Significant reduction of ChIs were found in DL quadrant only (Fig. 2F, CT and Ch2KO: $p = 0.016$; CT and DHet: $p = 0.34$; Ch2KO and DHet: $p = 0.022$, GENMOD with a gamma distribution). Furthermore, we measured the density of the striatal ChIs in 13-month-old mice. Similar to the 5-month group, *Dyt1* Ch2KO mice (n = 4) had similar striatal area size with the control mice (n = 3; Fig. 2H, $p = 0.54$, GENMOD with a gamma distribution). There was a significant reduction of both the number (Fig. 2G, $p < 0.001$, GENMOD with a gamma

distribution) and density (Fig. 2I, $p < 0.001$, GENMOD with a gamma distribution) of ChAT-positive neurons in the striatum of *Dyt1* Ch2KO mice. Interestingly, unlike the 5-month group, significant reduction of ChIs were found in all four quadrants in Ch2KO mice at 13 month of age (Fig. 2J, DL: $p < 0.001$; DM: $p = 0.022$; VL: $p = 0.010$; VM: $p < 0.001$, GENMOD with a gamma distribution).

3.3. Intrinsic membrane properties and responses to muscarine and quinpirole

We next evaluated the effect of selective knockout of torsinA in ChIs on intrinsic neuronal properties with whole-cell patch clamp recording. Passive membrane properties were measured in ChIs from both control and *Dyt1* Ch2KO mice (n = 6 each) voltage clamped at −70 mV. Selective *Dyt1* knockout did not alter input resistance (Fig. 3A, CT: n = 21 cells; Ch2KO: n = 17 cells, $p = 0.102$, student's t-test) or whole cell capacitance (Fig. 3B, CT: n = 21 cells; Ch2KO: n = 17 cells, $p = 0.361$, student's t-test) in ChIs, but was associated with significantly increased current density over a range of subthreshold voltages (Fig. 3C, current density at −70 mV, CT: n = 21 cells; Ch2KO: n = 18 cells, $p = 0.006$, student's t-test; Fig. 3D, main effect of torsinA knockout: F = 4.877, $p = 0.034$, repeated measures two-way ANOVA).

There was no change of resting membrane potential of ChIs in Ch2KO mice compared to the control mice (Fig. 3F, CT: n = 17 cells; Ch2KO: n = 17 cells, $p = 0.8084$, student's t-test). Action potential (AP) properties were measured with the first AP extracted during a slow current ramp protocol (Fig. 3E, See Methods). Overall, no significant difference was observed in rheobase, threshold, afterhyperpolarization amplitude, AP amplitude, AP width, maximal rate of depolarization or maximal rate of repolarization (Table 1). Furthermore, we calculated the effect of Ih on voltage observed during a −200 pA step (Fig. 3G) and found no change in Ch2KO mice (Fig. 3G and H, CT: n = 18 cells; Ch2KO: n = 16 cells, $p = 0.592$, student's t-test). Finally, we evaluated neuronal gain in both Ch2KO and control ChIs, using series of 300 ms-long current steps from −200 pA to +600 pA (each starting from I = 0 pA). Neuronal gain was similar in ChIs from control and Ch2KO mice (n = 17 in each group, Fig. 3I, no main effect of torsinA knockout: F = 0.03, $p = 0.87$, repeated measures two-way ANOVA), indicating unchanged excitability of the mutant ChIs.

Striatal ChIs have a feedback autoregulation mechanism by ACh through M2/M4 muscarinic acetylcholine receptors (mAChR) (Yan and Surmeier, 1996). However, such a mechanism is not present in *Dyt1* Ch1KO mice (Sciamanna et al., 2012). Therefore we measured the response of striatal ChIs in *Dyt1* Ch2KO mice to 10 μM muscarine using the cell-attached recording. Before the muscarine treatment, there was no significant difference in spontaneous AP frequency (Fig. 4A and B, CT: n = 13 cells; Ch2KO: n = 13 cells, $p = 0.52$, GENMOD with a gamma distribution) or coefficient of variation (CV; Fig. 4C, CV, CT: n = 13 cells; Ch2KO: n = 13 cells, $p = 0.15$, GENMOD with a gamma distribution) between *Dyt1* Ch2KO and control ChIs (n = 6 mice each). These results indicate that spontaneous firing activities were normal in the mutant striatal ChIs. After recording basal spontaneous activity, muscarine was applied, and the effect on the spontaneous firing was quantified. The ChIs from both the control and the *Dyt1* Ch2KO mice showed significantly decreased frequency after muscarine application (Fig. 4D and G, CT: n = 12 cells, $p < 0.001$; Ch2KO:

n = 12 cells, $p < 0.001$, GENMOD with a gamma distribution). Consistent with these observations, whole-cell voltage-clamp recording at −70 mV revealed that bath application of 10 μM muscarine induced an inhibitory outward current in both control (Fig. 4H, n = 8 cells, n = 5 mice, $p = 0.013$, paired two-sample t-test) and mutant ChIs (Fig. 4H, n = 11 cells, n = 5 mice, $p = 0.004$, one-sample t-test). Furthermore, the muscarine-mediated effect on current density was not different between Ch2KO and control ChIs ($p = 0.73$, student's t-test), indicating a similar inhibitory effect of muscarine in both groups. Finally, we tested the muscarine effect with the whole-cell current-clamp recording (Fig. 4E). We found muscarine-mediated inhibition in both CT (Fig. 4I, n = 10 cells, n = 3 mice, $p < 0.001$, GENMOD with a gamma distribution) and KO ChIs (Fig. 4I, n = 11 cells, n = 5 mice, $p < 0.001$, GENMOD with a gamma distribution). These results suggest that M2/M4 receptors are functionally intact in the Ch2KO ChIs.

Paradoxical excitation in response to D2R agonist quinpirole was reported in several DYT1 dystonia animal models, including *Dyt1* Ch1KO mice (Sciamanna et al., 2012). Therefore, the effect of quinpirole on ChIs was further examined (Fig. 4E). The control mice showed significantly decreased frequency after the quinpirole application (Fig. 4J, n = 16 cells, 6 mice, $p = 0.047$, GENMOD with a gamma distribution), and the ChIs recovered after the end of quinpirole treatment (Suppl. Fig. 1, n = 16 cells, 6 mice, $p = 0.31$, GENMOD with a gamma distribution). However, the mutant ChIs exhibited no such inhibition (Fig. 4J, n = 16 cells, 6 mice, $p = 0.16$, GENMOD with a gamma distribution). Nor was there any delayed effect (Suppl. Fig. 1, n = 16 cells, 6 mice, $p = 0.64$, GENMOD with a gamma distribution). The results suggest an altered response to quinpirole in Ch2KO mice.

3.4. Motor coordination and balance deficits and abnormal paw clenching

To investigate the general motor performance of *Dyt1* Ch2KO, we performed a series of behavioral tests. In the semi-quantitative assessments, there were no overt truncal arching, kyphosis, and unkempt fur in the Ch2KO mice (Fig. 5A). All mice exhibited strong righting reflexes when tipped on their side. In the open field test, *Dyt1* Ch2KO mice at 5 months of age exhibited no changes in horizontal (Fig. 5B, CT: n = 13 mice; Ch2KO: n = 13 mice; $p = 0.45$, GENMOD with a gamma distribution) and vertical movements (Fig. 5C, $p = 0.55$, Mixed model).

In the accelerated rotarod test, the mice were put on an accelerated rotarod and were tested for six trials over 2 days, and the latency to fall was measured. Ch2KO mice at 5 months of age had comparable results with their WT littermates in the rotarod test (Wilkes *et al.*, *in preparation*). However, The Ch2KO mice at 7-months-old showed a significantly shorter latency to fall when compared with the control group (Fig. 5D–E, CT: n = 11 mice; Ch2KO: n = 14 mice; $p = 0.05$, GENMOD with a gamma distribution). Motor coordination and balance were further analyzed by the beam-walking test. Like the rotarod test, Ch2KO mice at 5 months of age did not show significant beam-walking test deficits (Wilkes *et al.*, *in preparation*). On the other hand, the *Dyt1* Ch2KO mice at 9 months of age displayed a significant 83% increase of slips over the control group (Fig. 5F, CT: n = 11; Ch2KO: n = 14, $p = 0.02$, GENMOD with a negative binomial distribution). We further analyzed the motor learning in the beam-walking test by comparing the slip numbers at the first and

second trials (Fig. 5G, GENMOD with a negative binomial distribution). Although control mice improved significantly in trial 2 over trial 1 ($p = 0.05$), there was no significant difference between trials 1 and 2 for the Ch2KO mice ($p = 0.99$). Moreover, there was already a significant difference in trial 1 between Ch2KO and CT littermates ($p = 0.037$). Taken together, the *Dyt1* Ch2KO mice displayed deficits in motor coordination and balance, and motor learning.

Remarkably during the tail hang, Ch2KO mice at 13 months of age exhibited frequent paw clenching, without limb clasping (Fig. 5H–I). The severity of paw clenching was significantly higher in Ch2KO mice (Fig. 5H, CT: n = 11; Ch2KO: n = 14, $p = 0.05$, PLUM procedure). These results suggest that knockout of torsinA in ChIs is sufficient to produce motor coordination and balance deficits, and paw clenching.

4. Discussion

In this study, we developed and characterized a refined version of the ChI-specific *Dyt1* conditional knockout mouse model, Ch2KO. The Ch2KO mice had a reduced number of striatal ChIs in the dorsolateral striatum at 5 months of age and across the whole striatum at 13 months of age. Our electrophysiological studies revealed alterations in the current density and response to the quinpirole application, while the response to the muscarine was intact. The mutant mice exhibited increased paw clenching during the tail hang and additional motor deficits in the rotarod and beam-walking tests. Overall, these results indicate that knocking out torsinA in the ChI alone could lead to a reduced striatal ChI number and abnormal motor behaviors. Our results demonstrated a cell-autonomous effect of *Dyt1* deletion on the striatal ChIs and motor behavior, implicating the striatal ChIs in the pathogenesis of DYT1 dystonia.

Both the striatal ChAT expression and ChI density were reduced in *Dyt1* Ch2KO mice. A previous study did not find any changes in the number of striatal ChIs in the *Dyt1* Ch1KO mice (Sciamanna et al., 2012). On the other hand, studies with Dlx-CKO/ mice (Pappas et al., 2015) and ChAT-CKO/ mice (Pappas et al., 2018) showed a significant reduction of striatal ChIs in mutant mice. However, both these two lines not only inactivated *Dyt1* gene in the ChIs but also removed the other copy of the *Dyt1* gene throughout the whole body. How the heterozygous *Dyt1* knockout in the other cells contributes to the ChI loss found in the CKO/ mice is not clear. Here, the Ch2KO mouse model we developed had a reduced number of striatal ChIs in the absence of the heterozygous knockout of *Dyt1* or the ectopic *Ch1cre* expression, indicating that torsinA-related ChI loss was cell-autonomous.

A significant reduction of ChIs only occurs in the dorsal part of the striatum in the Dlx-CKO/ and ChAT-CKO/ mice (Pappas et al., 2015; Pappas et al., 2018), with the most prominent loss in the dorsolateral striatum. Interestingly, we found selective ChI reduction only in the dorsolateral striatum at 5 months of age. The dorsal striatum is critically involved in motor control in the brain, especially the dorsolateral subdivision. The dorsolateral striatum has been shown to regulate action sequences (O'Hare et al., 2018) and motor skill learning on the accelerating rotarod (Yin et al., 2009). On the other hand, we found significant reductions of ChIs in all 4 quadrants in the 13-month-old mutant mice,

suggesting that the neurodegeneration starts from the dorsolateral part and gradually extends to the rest of the striatum.

Consistent with the other reported rodent models of DYT1 dystonia (Dang et al., 2005; Dang et al., 2006; DeAndrade et al., 2016; Grundmann et al., 2012; Oleas et al., 2013; Page et al., 2010; Richter and Richter, 2014; Sciamanna et al., 2012; Sharma et al., 2005; Song et al., 2012; Yokoi et al., 2011; Yokoi et al., 2012; Yokoi et al., 2015b; Yokoi et al., 2008; Zhang et al., 2011; Zhao et al., 2008), *Dyt1* Ch2KO exhibited motor deficits in the rotarod and beam-walking tests, which are measurements of fine motor coordination and balance. Ch2KO mice also exhibited impaired motor learning, similar to the mice overexpressing human mutant torsinA (Grundmann et al., 2007; Sciamanna et al., 2011; Sharma et al., 2005). Furthermore, Ch2KO mice showed no changes in the open field test. In contrast, ChAT-CKO/ mice have hypoactivity. Ch2KO mice showed increased paw clenching at 13 months of age during the tail hang test but lacked trunk twisting, tremulousness, clasping, and kyphotic curvature in the spinal cord, which is present in the ChAT-CKO/ mice (Table 2). The additional deletion of one *Dyt1* allele in other cell types may contribute to the postural abnormalities and impaired behavioral performance of the ChAT-CKO/ mice.

Electrophysiological studies revealed functional changes of the striatal ChIs in the *Dyt1* Ch2KO mice. Contrary to the Ch1KO mice (Sciamanna et al., 2012), the Ch2KO mice did not show muscarine response changes, indicating M2/M4 receptors were functionally intact in the *Dyt1* Ch2KO ChIs. This discrepancy may be due to the ectopic *Ch1cre* expression in the *Dyt1* Ch1KO mice. Similar to the abnormal response reported in other DYT1 animal models (Eskow Jaunarajs et al., 2019; Grundmann et al., 2012; Martella et al., 2014; Scarduzio et al., 2017; Sciamanna et al., 2012; Sciamanna et al., 2011), the Ch2KO mice showed an impaired quinpirole response. The result highlights the importance of dopaminergic signaling in DYT1 dystonia pathophysiology (Downs et al., 2019). A previous study found that mutant torsinA results in a loss of function and can reduce the cell-surface localization of the polytopic membrane-bound proteins (Torres et al., 2004). Selective removal of torsinA in ChIs may lead to fewer D2R targeted to the membrane surface (Bonsi et al., 2019).

Analysis of genetic mouse models has contributed to the understanding of brain networks involved in the pathogenesis of DYT1 dystonia. The *Dyt1* GAG knock-in mice (Dang et al., 2005; Goodchild et al., 2005; Song et al., 2012), *Dyt1* knockdown mice (Dang et al., 2006), and *Dyt1* heterozygous knockout mice (Yokoi et al., 2015a) all have reduced torsinA levels and motor coordination and balance deficits, suggesting that mutant torsinA likely results in loss of function in DYT1 dystonia. Both *Dyt1* cerebral cortex-specific KO (*Dyt1* cKO) mice (Yokoi et al., 2008) and *Dyt1* striatum-specific KO (*Dyt1* sKO) mice (Yokoi et al., 2011) have motor deficits similar to the *Dyt1* knock-in mice, suggesting the importance of the corticostriatal pathway in the pathogenesis of DYT1 dystonia. Indeed, the corticostriatal long-term depression (LTD) was absent in the *Dyt1* GAG knock-in mice (Dang et al., 2012). The LTD deficit can be restored by anticholinergic trihexyphenidyl. The *Dyt1* sKO mice were generated using *Rgs9-cre* knock-in mice. We recently determined that the *Rgs9-cre*-mediated recombination is restricted to medium spiny neurons, and the striatal ChIs are spared (Lyu et al., 2019). Our results revealed that Ch2KO mice had reduced

number and altered intrinsic properties and quinpirole response of the striatal ChIs. The Ch2KO mice also had abnormal paw clenching and other motor deficits. The current study extended our striatum-specific knockout analysis to the ChIs. ChIs play an essential role in corticostriatal synaptic plasticity (Wang et al., 2006). The results from *Dyt1* cKO, sKO, and Ch2KO mice suggest that dysfunction of corticostriatal synapses is central to the pathogenesis of DYT1 dystonia. Pathophysiological changes caused by mutant torsinA in cortical projection neurons, medium spiny neurons, and striatal ChIs all contribute to the pathogenesis of DYT1 dystonia. The advances in genome engineering method, especially the clustered regularly interspaced short palindromic repeat/CRISPR associated protein 9 (CRISPR/Cas9) technology, has made it possible to correct *DYT1* mutation directly (Cruz et al., 2020). Our results suggest that a successful CRISPR/Cas9 gene therapy needs to target at least all three types of neurons in the corticostriatal pathway. Corticostriatal synaptic transmission is also regulated by striatal dopamine terminals from the substantia nigra and interneurons (Bamford et al., 2004; Calabresi et al., 2007). So far, no dopaminergic neuron-specific *Dyt1* knockout or ΔGAG knock-in mice have been characterized. Future studies of dopaminergic neurons and other striatal interneurons will reveal how mutant torsinA alters corticostriatal synaptic transmission and contribute to the development of newer, targeted therapy to cure DYT1 dystonia.

Supplementary Material

Refer to Web version on PubMed Central for supplementary material.

Acknowledgments

Abbreviations:

ACh	acetylcholine
***Ch1cre* mice**	*Chat-neo-cre* mice
***Ch2cre* mice**	*Chat-cre-Δneo* mice
ChAT	choline acetyltransferase
ChI	cholinergic interneuron
ChAT-CKO/− mice	*Chat-cre*-derived cholinergic neuron-specific KO in one allele and *Dyt1* KO in another allele mice

CRISPR/Cas9	clustered regularly interspaced short palindromic repeat/ CRISPR associated protein 9
CT	control
DHet	double heterozygote
Dlx-CKO/ mice	*Dlx-cre*-derived forebrain-specific KO in one allele and *Dyt1* KO in another allele mice
Dyt1 Ch1KO mice	*Dyt1* conditional knockout mice made from *Ch1cre* mice
Dyt1 Ch2KO mice	*Dyt1* conditional knockout mice made from *Ch2cre* mice
Dyt1 cKO	*Dyt1* cerebral cortex-specific KO mice
Dyt1 sKO	*Dyt1* striatum-specific KO mice
FIHC	fluorescence immunohistochemistry
GAPDH	Glyceraldehyde-3-phosphate dehydrogenase
GFP	green fluorescent protein
IHC	immunohistochemistry
KO	knockout
PB	phosphate buffer

References

Albanese A, et al., 2013. Phenomenology and classification of dystonia: a consensus update. Mov Disord. 28, 863–73. [PubMed: 23649720]

Aosaki T, et al., 2010. Acetylcholine-dopamine balance hypothesis in the striatum: an update. Geriatr Gerontol Int. 10 Suppl 1, S148–57. [PubMed: 20590830]

Augood SJ, et al., 1999. Distribution of the mRNAs encoding torsinA and torsinB in the normal adult human brain. Ann Neurol. 46, 761–9. [PubMed: 10553994]

Bamford NS, et al., 2004. Dopamine modulates release from corticostriatal terminals. J Neurosci. 24, 9541–52. [PubMed: 15509741]

Bonsi P, et al., 2019. RGS9–2 rescues dopamine D2 receptor levels and signaling in DYT1 dystonia mouse models. EMBO Mol Med. 11.

Bressman SB, et al., 2000. The DYT1 phenotype and guidelines for diagnostic testing. Neurology. 54, 1746–52. [PubMed: 10802779]

Brown RS, et al., 2014. The mechanism of Torsin ATPase activation. Proc Natl Acad Sci U S A. 111, E4822–31. [PubMed: 25352667]

Calabresi P, et al., 2007. Dopamine-mediated regulation of corticostriatal synaptic plasticity. Trends Neurosci. 30, 211–9. [PubMed: 17367873]

Chase AR, et al., 2017. Torsin ATPases: Harnessing Dynamic Instability for Function. Front Mol Biosci. 4, 29. [PubMed: 28553638]

Chuhma N, et al., 2014. Dopamine neurons control striatal cholinergic neurons via regionally heterogeneous dopamine and glutamate signaling. Neuron. 81, 901–12. [PubMed: 24559678]

Cirino T, et al., 2020. Region-specific effects of HIV-1 Tat on intrinsic electrophysiological properties of pyramidal neurons in mouse prefrontal cortex and hippocampus. Journal of neurophysiology. 123.

Cruz L, et al., 2020. Mutant Allele-Specific CRISPR Disruption in DYT1 Dystonia Fibroblasts Restores Cell Function. Molecular therapy. Nucleic acids 21.

Dang MT, et al., 2012. An anticholinergic reverses motor control and corticostriatal LTD deficits in Dyt1 DeltaGAG knock-in mice. Behav Brain Res. 226, 465–72. [PubMed: 21995941]

Dang MT, et al., 2005. Generation and characterization of Dyt1 DeltaGAG knock-in mouse as a model for early-onset dystonia. Exp Neurol. 196, 452–63. [PubMed: 16242683]

Dang MT, et al., 2006. Motor deficits and hyperactivity in Dyt1 knockdown mice. Neurosci Res. 56, 470–4. [PubMed: 17046090]

DeAndrade MP, et al., 2012. Motor restlessness, sleep disturbances, thermal sensory alterations and elevated serum iron levels in Btbd9 mutant mice. Hum Mol Genet. 21, 3984–92. [PubMed: 22678064]

DeAndrade MP, et al., 2016. Electromyographic evidence in support of a knock-in mouse model of DYT1 Dystonia. Mov Disord. 31, 1633–1639. [PubMed: 27241685]

Demircioglu FE, et al., 2016. Structures of TorsinA and its disease-mutant complexed with an activator reveal the molecular basis for primary dystonia. Elife. 5.

Ding J, et al., 2006. RGS4-dependent attenuation of M4 autoreceptor function in striatal cholinergic interneurons following dopamine depletion. Nat Neurosci. 9, 832–42. [PubMed: 16699510]

Downs AM, et al., 2019. Trihexyphenidyl rescues the deficit in dopamine neurotransmission in a mouse model of DYT1 dystonia. Neurobiol Dis. 125, 115–122. [PubMed: 30707939]

Eskow Jaunarajs K, et al., 2019. Diverse Mechanisms Lead to Common Dysfunction of Striatal Cholinergic Interneurons in Distinct Genetic Mouse Models of Dystonia. The Journal of neuroscience : the official journal of the Society for Neuroscience. 39.

Eskow Jaunarajs KL, et al., 2015. Striatal cholinergic dysfunction as a unifying theme in the pathophysiology of dystonia. Prog Neurobiol. 127–128, 91–107.

Farley FW, et al., 2000. Widespread recombinase expression using FLPeR (flipper) mice. Genesis. 28, 106–10. [PubMed: 11105051]

Fernagut PO, et al., 2002. Subacute systemic 3-nitropropionic acid intoxication induces a distinct motor disorder in adult C57Bl/6 mice: behavioural and histopathological characterisation. Neuroscience. 114, 1005–17. [PubMed: 12379255]

Franklin K, Paxinos G, The mouse brain in stereotaxic coordinates. Elsevier Academic Press, 2008.

Golowasch J, et al., 2009. Membrane capacitance measurements revisited: dependence of capacitance value on measurement method in nonisopotential neurons. J Neurophysiol. 102, 2161–75. [PubMed: 19571202]

Goodchild RE, et al., 2005. Loss of the dystonia-associated protein torsinA selectively disrupts the neuronal nuclear envelope. Neuron. 48, 923–32. [PubMed: 16364897]

Grundmann K, et al., 2012. Generation of a novel rodent model for DYT1 dystonia. Neurobiol Dis. 47, 61–74. [PubMed: 22472189]

Grundmann K, et al., 2007. Overexpression of human wildtype torsinA and human DeltaGAG torsinA in a transgenic mouse model causes phenotypic abnormalities. Neurobiol Dis. 27, 190–206. [PubMed: 17601741]

Hedrick T, et al., 2016. Characterization of Channelrhodopsin and Archaerhodopsin in Cholinergic Neurons of Cre-Lox Transgenic Mice. PloS one. 11, e0156596. [PubMed: 27243816]

Howe AR, Surmeier DJ, 1995. Muscarinic receptors modulate N-, P-, and L-type Ca2+ currents in rat striatal neurons through parallel pathways. J Neurosci. 15, 458–69. [PubMed: 7823150]

Isik E, et al., 2019. Biallelic TOR1A mutations cause severe arthrogryposis: A case requiring reverse phenotyping. Eur J Med Genet. 62, 103544. [PubMed: 30244176]

Jankovic J, 2013. Medical treatment of dystonia. Mov Disord. 28, 1001–12. [PubMed: 23893456]

Kariminejad A, et al., 2017. TOR1A variants cause a severe arthrogryposis with developmental delay, strabismus and tremor. Brain. 140, 2851–2859. [PubMed: 29053766]

Kock N, et al., 2006. Effects of genetic variations in the dystonia protein torsinA: identification of polymorphism at residue 216 as protein modifier. Hum Mol Genet. 15, 1355–64. [PubMed: 16537570]

Konakova M, Pulst SM, 2005. Dystonia-associated forms of torsinA are deficient in ATPase activity. J Mol Neurosci. 25, 105–17. [PubMed: 15781971]

Liang CC, et al., 2014. TorsinA hypofunction causes abnormal twisting movements and sensorimotor circuit neurodegeneration. J Clin Invest. 124, 3080–92. [PubMed: 24937429]

Lyu S, et al., 2019. The role of BTBD9 in striatum and restless legs syndrome. eNeuro. 0277–19.

Madisen L, et al., 2010. A robust and high-throughput Cre reporting and characterization system for the whole mouse brain. Nat Neurosci. 13, 133–40. [PubMed: 20023653]

Marras C, et al., 2016. Nomenclature of genetic movement disorders: Recommendations of the international Parkinson and movement disorder society task force. Mov Disord. 31, 436–57. [PubMed: 27079681]

Martella G, et al., 2014. Regional specificity of synaptic plasticity deficits in a knock-in mouse model of DYT1 dystonia. Neurobiol Dis. 65, 124–32. [PubMed: 24503369]

Maurice N, et al., 2004. D2 dopamine receptor-mediated modulation of voltage-dependent Na+ channels reduces autonomous activity in striatal cholinergic interneurons. J Neurosci. 24, 10289–301. [PubMed: 15548642]

Nasirova N, et al., 2020. Dual recombinase fate mapping reveals a transient cholinergic phenotype in multiple populations of developing glutamatergic neurons. The Journal of comparative neurology. 528, 283–307. [PubMed: 31396962]

O'Hare J, et al., 2018. Recent Insights into Corticostriatal Circuit Mechanisms underlying Habits: Invited review for Current Opinions in Behavioral Sciences. Current opinion in behavioral sciences. 20.

Oleas J, et al., 2013. Engineering animal models of dystonia. Mov Disord. 28, 990–1000. [PubMed: 23893455]

Opal P, et al., 2002. Intrafamilial phenotypic variability of the DYT1 dystonia: from asymptomatic TOR1A gene carrier status to dystonic storm. Mov Disord. 17, 339–45. [PubMed: 11921121]

Oswald M, et al., 2009. IH current generates the afterhyperpolarisation following activation of subthreshold cortical synaptic inputs to striatal cholinergic interneurons. The Journal of physiology. 587.

Ozelius LJ, et al., 1997. The early-onset torsion dystonia gene (DYT1) encodes an ATP-binding protein. Nat Genet. 17, 40–8. [PubMed: 9288096]

Page ME, et al., 2010. Cell-autonomous alteration of dopaminergic transmission by wild type and mutant (DeltaE) TorsinA in transgenic mice. Neurobiol Dis. 39, 318–26. [PubMed: 20460154]

Pappas SS, et al., 2015. Forebrain deletion of the dystonia protein torsinA causes dystonic-like movements and loss of striatal cholinergic neurons. Elife. 4, e08352. [PubMed: 26052670]

Pappas SS, et al., 2018. A cell autonomous torsinA requirement for cholinergic neuron survival and motor control. Elife. 7, e36691. [PubMed: 30117805]

Pham P, et al., 2006. Molecular defects of the dystonia-causing torsinA mutation. Neuroreport. 17, 1725–8. [PubMed: 17047461]

Pisani A, et al., 2007. Re-emergence of striatal cholinergic interneurons in movement disorders. Trends Neurosci. 30, 545–53. [PubMed: 17904652]

Reichert SC, et al., 2017. Biallelic TOR1A variants in an infant with severe arthrogryposis. Neurol Genet. 3, e154. [PubMed: 28516161]

Richter F, Richter A, 2014. Genetic animal models of dystonia: common features and diversities. Prog Neurobiol. 121, 91–113. [PubMed: 25034123]

Risch N, et al., 1995. Genetic analysis of idiopathic torsion dystonia in Ashkenazi Jews and their recent descent from a small founder population. Nat Genet. 9, 152–9. [PubMed: 7719342]

Rossi J, et al., 2011. Melanocortin-4 receptors expressed by cholinergic neurons regulate energy balance and glucose homeostasis. Cell Metab. 13, 195–204. [PubMed: 21284986]

Scarduzio M, et al., 2017. Strength of cholinergic tone dictates the polarity of dopamine D2 receptor modulation of striatal cholinergic interneuron excitability in DYT1 dystonia. Exp Neurol. 295, 162–175. [PubMed: 28587876]

Sciamanna G, et al., 2012. Cholinergic dysregulation produced by selective inactivation of the dystonia-associated protein torsinA. Neurobiol Dis. 47, 416–27. [PubMed: 22579992]

Sciamanna G, et al., Developmental Profile of the Aberrant Dopamine D2 Receptor Response in Striatal Cholinergic Interneurons in DYT1 Dystonia. PLoS One, 2011.

Sharma N, et al., 2005. Impaired motor learning in mice expressing torsinA with the DYT1 dystonia mutation. J Neurosci. 25, 5351–5. [PubMed: 15930383]

Shashidharan P, et al., 2000. Immunohistochemical localization and distribution of torsinA in normal human and rat brain. Brain Res. 853, 197–206. [PubMed: 10640617]

Siegert S, et al., 2005. TorsinA expression is detectable in human infants as young as 4 weeks old. Brain Res Dev Brain Res. 157, 19–26. [PubMed: 15939081]

Song CH, et al., 2012. Functional Analysis of Dopaminergic Systems in a DYT1 Knock-in Mouse Model of Dystonia. Neurobiol Dis. 48, 66–78. [PubMed: 22659308]

Stoof JC, et al., 1992. Regulation of the activity of striatal cholinergic neurons by dopamine. Neuroscience. 47, 755–70. [PubMed: 1579210]

Torres GE, et al., 2004. Effect of torsinA on membrane proteins reveals a loss of function and a dominant-negative phenotype of the dystonia-associated DeltaE-torsinA mutant. Proc Natl Acad Sci U S A. 101, 15650–5. [PubMed: 15505207]

Vasudevan A, et al., 2006. Developmental patterns of torsinA and torsinB expression. Brain Res. 1073–1074, 139–45.

Wang Z, et al., 2006. Dopaminergic control of corticostriatal long-term synaptic depression in medium spiny neurons is mediated by cholinergic interneurons. Neuron. 50, 443–52. [PubMed: 16675398]

Xiao J, et al., 2004. Developmental expression of rat torsinA transcript and protein. Brain Res Dev Brain Res. 152, 47–60. [PubMed: 15283994]

Yan Z, Surmeier DJ, 1996. Muscarinic (m2/m4) receptors reduce N- and P-type Ca2+ currents in rat neostriatal cholinergic interneurons through a fast, membrane-delimited, G-protein pathway. J Neurosci. 16, 2592–604. [PubMed: 8786435]

Yin H, et al., 2009. Dynamic reorganization of striatal circuits during the acquisition and consolidation of a skill. Nature neuroscience. 12.

Yokoi F, et al., 2015a. Behavioral and electrophysiological characterization of Dyt1 heterozygous knockout mice. PLoS One. 10, e0120916. [PubMed: 25799505]

Yokoi F, et al., 2011. Motor deficits and decreased striatal dopamine receptor 2 binding activity in the striatum-specific Dyt1 conditional knockout mice. PLoS One. 6, e24539. [PubMed: 21931745]

Yokoi F, et al., 2012. Improved motor performance in Dyt1 DeltaGAG heterozygous knock-in mice by cerebellar Purkinje-cell specific Dyt1 conditional knocking-out. Behav Brain Res. 230, 389–98. [PubMed: 22391119]

Yokoi F, et al., 2015b. Decreased dopamine receptor 1 activity and impaired motor-skill transfer in Dyt1 DeltaGAG heterozygous knock-in mice. Behav Brain Res. 279, 202–10. [PubMed: 25451552]

Yokoi F, et al., 2008. Motor deficits and hyperactivity in cerebral cortex-specific Dyt1 conditional knockout mice. J Biochem. 143, 39–47. [PubMed: 17956903]

Yokoi F, et al., 2020. Decreased number of striatal cholinergic interneurons and motor deficits in dopamine receptor 2-expressing-cell-specific Dyt1 conditional knockout mice. Neurobiol Dis. 134, 104638. [PubMed: 31618684]

Yokoi F, et al., 2010. Earlier onset of motor deficits in mice with double mutations in Dyt1 and Sgce. J Biochem. 148, 459–66. [PubMed: 20627944]

Zambelli D, et al., 2012. Validation of a model to develop a symptom index for benign prostatic hyperplasia in dogs. Reprod Domest Anim. 47 Suppl 6, 229–31. [PubMed: 23279506]

Zhang L, et al., 2011. Altered dendritic morphology of Purkinje cells in Dyt1 DeltaGAG knock-in and purkinje cell-specific Dyt1 conditional knockout mice. PLoS One. 6, e18357. [PubMed: 21479250]

Zhao C, et al., 2013. Regulation of Torsin ATPases by LAP1 and LULL1. Proc Natl Acad Sci U S A. 110, E1545–54. [PubMed: 23569223]

Zhao Y, et al., 2008. Abnormal motor function and dopamine neurotransmission in DYT1 DeltaGAG transgenic mice. Exp Neurol. 210, 719–30. [PubMed: 18299128]

Highlights

- *Dyt1* Ch2KO mice had a reduced number of striatal cholinergic interneurons.

- *Dyt1* Ch2KO mice had paw clenching and deficits in rotarod and beam-walking tests.

- Mutant cholinergic interneurons had a normal response to the muscarine.

- Mutant cholinergic interneurons had an impaired response to the quinpirole.
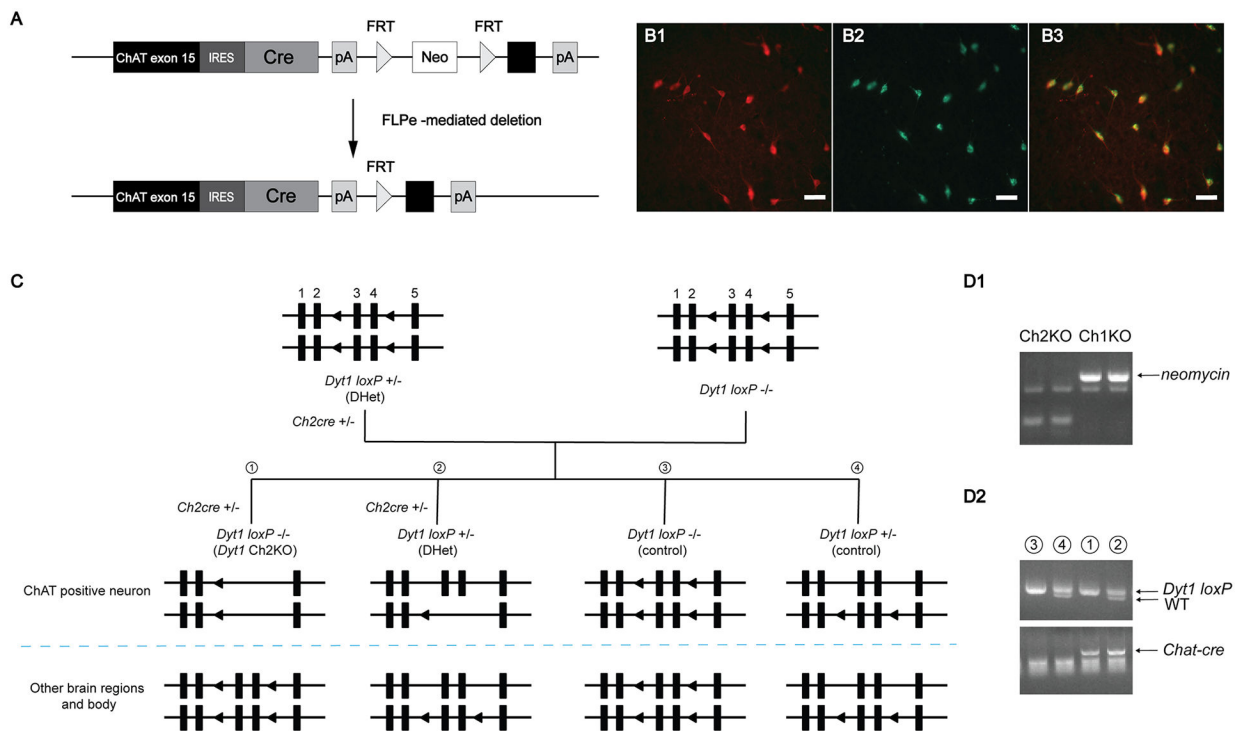
FIG 1. Generation of *Dyt1* Ch2KO mice.
(A) Schematic diagram of the generation of *Ch2cre* mice, modified from Fig. 1A in (Rossi et al., 2011). *Ch1cre* mice were crossed with FLP mice to remove the neomycin cassette to generate *Ch2cre* mice. (B) Representative fluorescence immunohistochemical images of the ChIs in *Ch2cre*-GFP mice. (B1) Striatal ChIs stained with the ChAT antibody. Fluorescence of GFP indicates *Ch2cre* recombinase activity (B2) and merged image (B3). Scale bar: 25 μm. (C) Schematic diagram of the generation of Ch2KO mice. Filled boxes represent exons. Filled triangles indicate *loxP* sites flanking the 3rd and 4th exon of the *Dyt1* gene. *Dyt1^{loxP}* mice were crossed with *Ch2cre* mice to obtain double heterozygotes (DHet). The DHet were crossed with *Dyt1^{loxP}* homozygotes to get *Dyt1* Ch2KO mice. In *Dyt1* Ch2KO mice, exons 3 and 4 were deleted in specific ChIs where *cre* is expressed, while other cell types/brain regions and the rest of the body were not affected. PCR reaction to confirm the removal of *neomycin* in *Dyt1* Ch2KO mice (D1) and the representative gel image of genotyping results. Lane 1: *Dyt1* Ch2KO mice. Lane 2: DHet mice. Lane 3: *Dyt1^{loxP}* homozygous mice. Lane 4: *Dyt1^{loxP}* heterozygous mice.
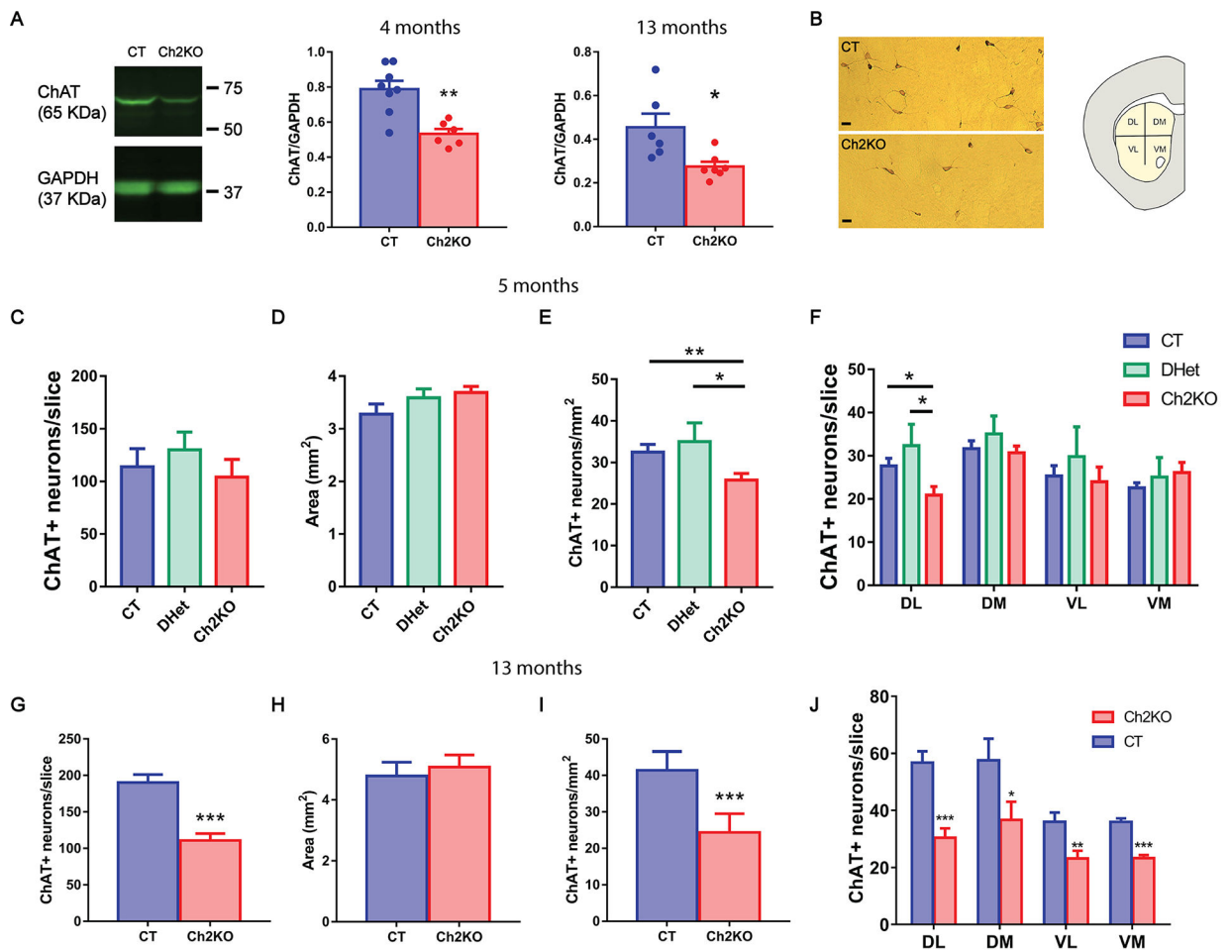
FIG 2. Decreased striatal ChAT protein level and reduced density of striatal ChIs in *Dyt1* Ch2KO mice.

(A) Representative Western blot images of striatal ChAT and its loading controls (GAPDH) are shown. The quantified protein bands were standardized to the GAPDH. A significant reduction of ChAT protein levels was found in the 4-month-old and 13-month-old *Dyt1* Ch2KO mice compared with their CT littermates. (B) Representative immunohistochemical images of the striatal ChAT-positive ChIs in CT and Ch2KO mice. Scale bar: 25 μm. (C-F) Quantification of the number of striatal ChAT-positive neurons in 5-month-old *Dyt1* Ch2KO mice. Reduced densities (E) of ChAT positive neurons are shown in Ch2KO mice compared with DHet and CT littermates, while the areas of the striatum (D) were unchanged. A significant reduction of ChI was found in dorsolateral (DL) striatum only (F). (G-J) Quantification of the number of striatal ChAT-positive neurons in 13-month-old *Dyt1* Ch2KO mice. Reduced numbers (G) and densities (I) of ChAT positive neurons are shown in KO mice compared with CT littermates. The areas of the striatum (H) were unchanged. A significant reduction of ChI was seen in every striatal quadrant: dorsolateral (DL), dorsomedial (DM), ventral lateral (VL) and ventral medial (VM) striatum (J). The bar graphs show mean ± standard errors of ChIs/slice. *p 0.05, **p 0.01, ***p 0.001.
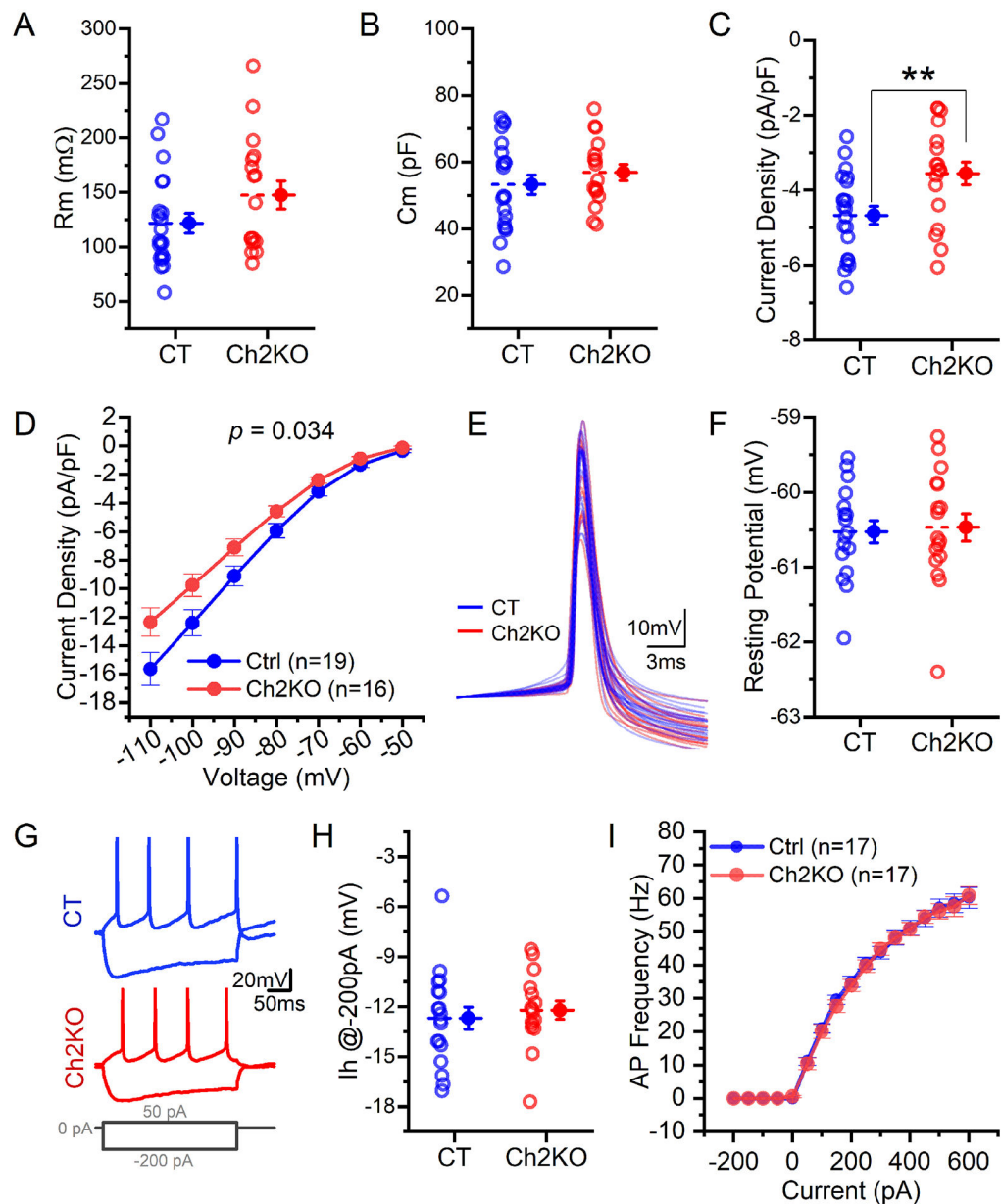
FIG 3. Passive and active properties of ChIs from CT and *Dyt1* Ch2KO mice.

ChIs from *Dyt1* Ch2KO mice displayed no changes in input resistance (Rm) or whole-cell capacitance, as measured at −70 mV, however, significant differences in current density were observed (C, D, see results for additional details). (E) The first action potential (AP) of each examined ChI extracted during a slow current ramp. Each action potential trace is baseline subtracted to a 1-msec period that occurred 10 msec before the action potential peak. (F) Resting potential of ChIs in *Dyt1* Ch2KO mice did not differ from that observed in ChIs of control littermates. (G) Representative voltage traces from both control and Ch2KO ChIs as observed in response to either −200 pA or 50 pA current injection. (H) Ih-mediated voltage change as observed during a −200 pA step was not different between CT and *Dyt1* Ch2KO

ChIs. (I) Action potential gain function was not different between CT and *Dyt1* Ch2KO ChIs. The bar graphs show mean ± standard errors. **p 0.01.
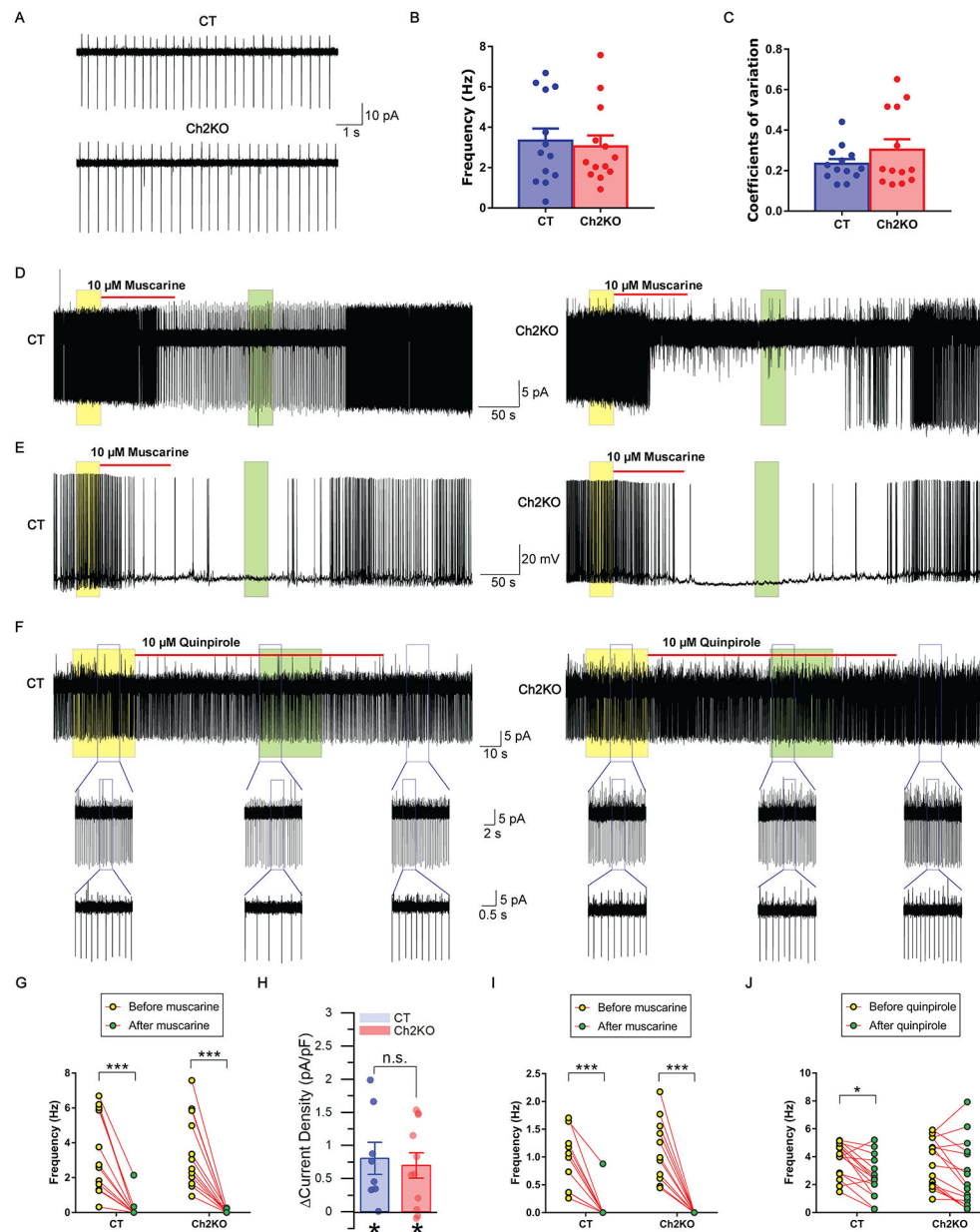
FIG 4. Responses to muscarine and quinpirole.

(A) Representative cell-attached recording traces of spontaneous action potentials of ChIs in *Dyt1* Ch2KO and CT mice. Both spontaneous action potential frequency (B) and coefficients of variation (C) were not changed between *Dyt1* Ch2KO and CT ChIs. Representative traces of spontaneous action potentials in *Dyt1* Ch2KO and CT mice in response to the application of 10 μM muscarine (D) or 10 μM quinpirole (F) under cell-attached recording configuration. (E) Representative traces of firing activities in *Dyt1* Ch2KO and CT mice in response to the application of 10 μM muscarine under whole-cell current-clamp configuration. Muscarine reduced the spontaneous action potential frequency in the ChIs from both the *Dyt1* Ch2KO and the CT littermates in both cell-attached (G) and whole-cell recordings (I). AP frequency was quantified 30 seconds before muscarine

application (yellow dots) and 180–210 seconds after the onset of muscarine application (green dots). (H) 10 μM muscarine induced an outward current in ChIs voltage clamped at −70 mV in whole-cell configuration in cells from both the CT and the *Dyt1* Ch2KO littermates. (J) 10 μM quinpirole reduced the spontaneous action potential frequency in ChIs from CT littermates but had no effect in the *Dyt1* Ch2KO mice. AP frequency was quantified 30 seconds before quinpirole application (shaded yellow) and 60–90 seconds after the onset of quinpirole application (shaded green). The bar graphs show mean ± standard errors. $*p < 0.05$, $***p < 0.001$.
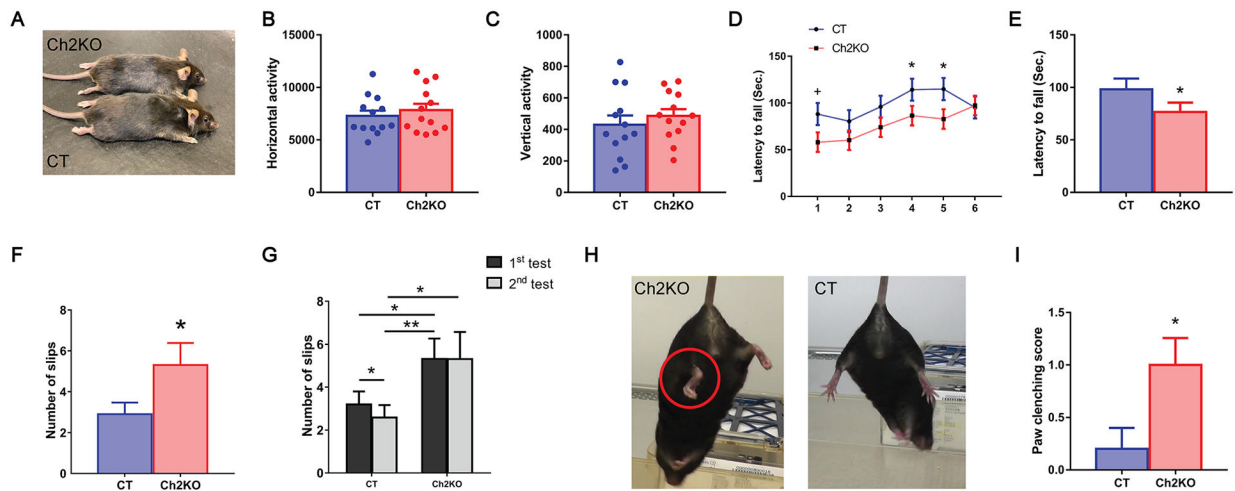
FIG 5.

Motor behavioral deficits in *Dyt1* Ch2KO mice. (A) Normal appearance and shape of the spinal cord in control and Ch2KO mice. Ch2KO mice showed normal performance in the open field in both horizontal movement (B) and vertical rearing (C) compared with CT mice. Ch2KO mice exhibited reduced latency to fall in the accelerated rotarod test compared with CT mice (D, E). 1 – 6: trial number. Ch2KO mice had excessive slips (F) on the beam-walking test. (G) Ch2KO had more slips in the first test and did not improve their performance in the second test compared to their CT littermates. (H) Paw clenching in a Ch2KO mouse. (I) The semi-quantitative analysis showed the paw clenching was prominent in *Dyt1* Ch2KO mice compared to control mice. Bars represent mean ± SEM. + p 0.1, *p 0.05, **p 0.01.

Table 1.

Action potential properties of ChIs

Animal (N)	Rheobase (pA)	Threshold (mV)	AHP Amplitude (mV)	AP Amplitude (mV)	AP Width (ms)	Repolarization Rate Max (V/s)	Depolarization Rate Max (V/s)
CT (6)	64.3 ± 4.9 (20)	−39.0 ± 0.8 (19)	−12.4 ± 0.9 (20)	56.3 ± 2.0 (20)	1.29 ± 0.03 (19)	−39.8 ± 2.1 (20)	94.3 ± 5.2 (20)
Ch2KO (6)	50.1 ± 7.0 (17)	−40.8 ± 0.9 (16)	−14.1 ± 0.7 (17)	54.4 ± 2.4 (18)	1.36 ± 0.03 (17)	−35.0 ± 1.7 (17)	87.1 ± 5.3 (18)

AP, action potential; AHP, afterhyperpolarization; The AP properties were calculated from the first AP produced in response to a slow current ramp. AP width, depolarization rate max and repolarization rate max were measured from the first derivative of the action potential. Values are displayed as mean ± s.e.m. N-values are provided in parentheses, and represent cell number, except in first column, where they represent number of animals.
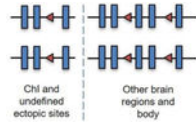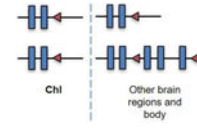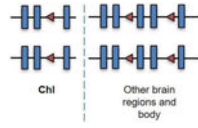
Table 2.

Comparison of *Dyt1* Ch1KO, ChAT-CKO/ and *Dyt1* Ch2KO mice.

Phenotype	*Dyt1* Ch1KO	ChKO/	*Dyt1* Ch2KO
TorsinA manipulation			
***Chat-cre* line**	*Ch1cre* mice	*Ch1cre* mice	*Ch2cre* mice
Tail hang	Normal	Twisting and tremulousness	Paw clenching
Open field	Normal	Hypoactivity	Normal
Rotarod	Reduced latency to fall	Normal	Reduced latency to fall
Beam-walking	Normal	NA	Excessive slips
Kyphosis	No	Yes	No
Response to muscarinic receptor activation	Altered	NA	Normal
Reduced number of striatal ChIs	No	Yes	Yes
The topographic pattern of ChI reduction	NA	Yes	Yes at 5 months NO at 13 months